Geophysical Research Letters

RESEARCH LETTER
10.1029/2025GL116605

Assessing Occurrence Patterns of Shallow Hikurangi Slow Slip Events Using Renewal Processes

Andrea Perez-Silva[1,2], Ting Wang[1], Laura Wallace[3,4,5], Mark Bebbington[6], and Paul Denys[1]

[1]University of Otago, Dunedin, New Zealand, [2]Now at GFZ Helmholtz Centre for Geosciences, Potsdam, Germany, [3]GEOMAR Helmholtz Center for Ocean Research Kiel, Kiel, Germany, [4]Institute of Geosciences, Christian-Albrechts-Universität zu Kiel, Kiel, Germany, [5]University of Texas Institute of Geophysics, Austin, TX, USA, [6]School of Mathematical and Computational Sciences, and School of Agriculture and Environment, Massey University, Palmerston North, New Zealand

Key Points:

- We constrain timing and length of slow slip events (SSEs) along shallow Hikurangi margin. Our catalog comprises 92 SSEs from 2006 to 2024
- We model SSE occurrence patterns as a marked renewal process and apply Bayesian methods for inference
- SSE recurrence interval and periodicity vary along the margin. SSEs have shorter recurrence times and more regular periodicity in the north

Supporting Information:

Supporting Information may be found in the online version of this article.

Correspondence to:

T. Wang,
ting.wang@otago.ac.nz

Citation:

Perez-Silva, A., Wang, T., Wallace, L., Bebbington, M., & Denys, P. (2025). Assessing occurrence patterns of shallow Hikurangi slow slip events using renewal processes. *Geophysical Research Letters*, *52*, e2025GL116605. https://doi.org/10.1029/2025GL116605

Received 18 APR 2025
Accepted 10 JUN 2025

Author Contributions:

Conceptualization: Andrea Perez-Silva, Ting Wang, Laura Wallace
Data curation: Andrea Perez-Silva
Formal analysis: Andrea Perez-Silva
Funding acquisition: Ting Wang
Investigation: Andrea Perez-Silva
Methodology: Andrea Perez-Silva, Ting Wang, Laura Wallace, Mark Bebbington
Project administration: Ting Wang
Software: Andrea Perez-Silva, Ting Wang
Supervision: Ting Wang, Laura Wallace
Validation: Andrea Perez-Silva, Laura Wallace, Paul Denys
Visualization: Andrea Perez-Silva

Abstract We investigate the occurrence patterns of SSEs along the shallow (<15 km) portion of the Hikurangi subduction zone. First, we build a manual catalog constraining timing and length of 92 SSEs between 2006 and 2024. Then, we investigate SSE occurrence patterns by fitting a renewal process, using Bayesian inference to obtain the posterior distribution of model parameters. Our results show that SSE recurrence intervals vary along the Hikurangi margin; less frequent SSEs occur in the southern part of the margin. The periodicity of SSEs also changes along strike. SSEs in the northern part of the margin occur more regularly than those at the central part. Finally, we do not find conclusive evidence that 2016 M_w7.8 Kaikōura earthquake had a lasting effect on SSE occurrence patterns.

Plain Language Summary Slow slip events (SSEs), which have slower velocities and longer durations than regular earthquakes, have been detected at several subduction zones worldwide. Here, we investigate the occurrence patterns of these events, that is how often they occur and how periodic is their behavior, among other characteristics. We focus on SSEs that occur in the North Island of New Zealand, along the shallow portion of the Hikurangi subduction zone, which marks the subduction of the Pacific Plate beneath the Australian plate. First, we build a manual catalog of these SSEs and identify 92 events between 2006 and 2024. Using a statistical model for the timing and size of SSEs, we estimate characteristics such as the recurrence interval and periodicity. Our results indicate that SSEs occur less frequently in the southern part of the margin. We also find that they occur more regularly in the northern part of the margin. We examined the occurrence patterns of SSEs before and after Kaikōura earthquake, which was a large (M_w7.8) earthquake that struck New Zealand's northeastern South Island. However, we did not find conclusive evidence of a lasting effect of the earthquake on SSE occurrence patterns.

1. Introduction

Slow slip events (SSEs) are transient episodes of aseismic slip with longer durations and slower slip speeds than regular earthquakes. These events have been observed in various tectonic environments (e.g., B. Brooks et al., 2006; Hirose et al., 1999; Rousset et al., 2017, 2019; Wei et al., 2009), but they are most commonly detected in subduction zones (e.g., Dixon et al., 2014; Dragert et al., 2001; Fu et al., 2015; Graham et al., 2016). Perhaps the most striking characteristic of SSEs, which sets them apart from regular earthquakes, is their occurrence patterns. Ample evidence shows that SSE occur at fairly regular periods, with recurrence intervals ranging from tens of days to several years (e.g., Nishimura, 2014; Radiguet et al., 2012; Takagi et al., 2019). Despite their regularity, SSE recurrence period may vary along-strike and/or along-depth within a given subduction zone (e.g., Audet & Bürgmann, 2014; Brudzinski & Allen, 2007; Fu et al., 2015; Takagi et al., 2019), and earthquake occurrence may also affect their timing (Cruz-Atienza et al., 2021; Ozawa, 2014). These characteristics suggest that SSE occurrence patterns are far from simple.

Characterizing SSE occurrence patterns is fundamental to understand their behavior and to assess whether they can be forecast. A quantitative description of SSE patterns is also necessary to detect anomalous behavior caused by external factors, such as large earthquakes. Renewal processes are commonly used to model the occurrence patterns of geological events, such as volcanic eruptions (Bebbington & Lai, 1996; Cruz-Reyna & Carrasco-Núñez, 2002; Wang & Bebbington, 2012; Wang et al., 2022), large earthquakes (Matthews et al., 2002; Nomura

Writing – original draft: Andrea Perez-Silva
Writing – review & editing: Andrea Perez-Silva, Ting Wang, Laura Wallace, Mark Bebbington, Paul Denys

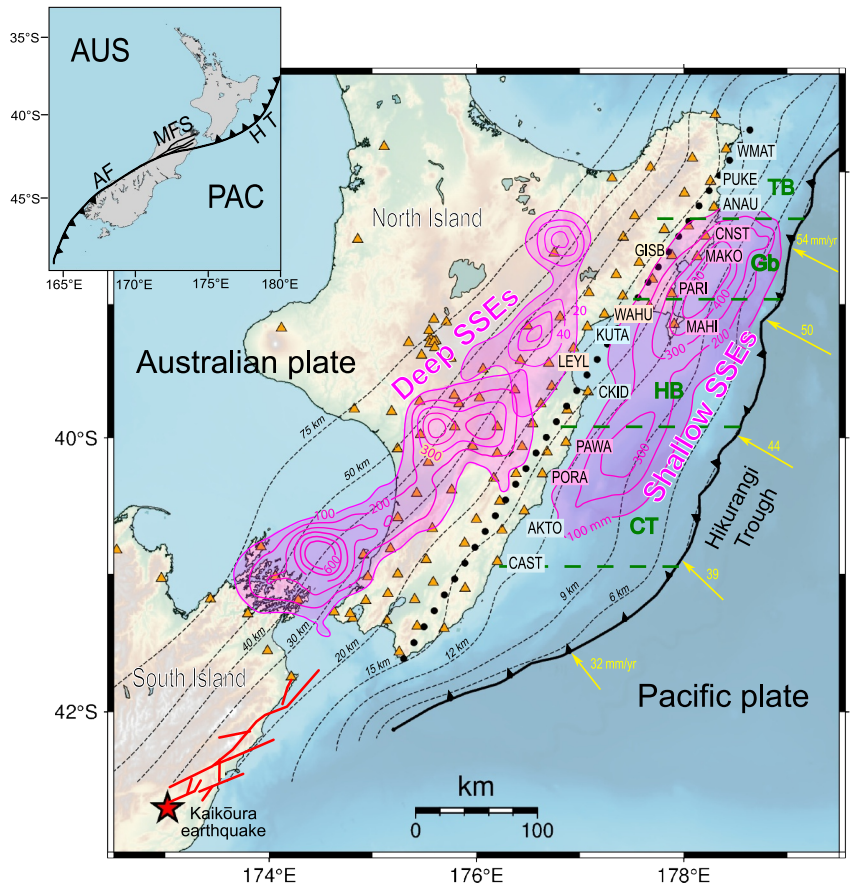

Figure 1. Main panel shows the tectonic setting of the Hikurangi margin. Magenta contours show cumulative slip (in mm) of shallow and deep SSEs between 2002 and 2014 (Wallace, 2020). Orange triangles show the location of continuous GPS stations from the GeoNet network. Labels are included for stations closest to the coast. Yellow arrows indicate the plate convergence rate in mm/yr (Wallace, Barnes, et al., 2012). Dashed black lines are the depth contour (below sea level) of the subducting plate interface (Williams et al., 2013). Black circles show the transect along which we project SSE detections (Section 2). Dashed green horizontal lines indicate the segments into which the margin is divided, which correspond to Tolaga Bay (TB), Gisborne (Gb), Hawkes Bay (HB) and Cape Turnagain (CT, Section 3.1). Red star shows the epicentral location of 2016 M_w7.8 Kaikōura earthquake. Red lines show the surface traces of faults that ruptured in the earthquake (Hamling et al., 2017). Inset, regional tectonic framework showing Pacific (PAC) and Australian (AUS) plates. HT stands for Hikurangi Trough, MFS for Malborough fault system and AF for Alpine Fault.

et al., 2011; Ogata, 1999; Wang et al., 2024) and tectonic tremors (Ide & Nomura, 2022) —a phenomenon closely related to SSEs (e.g., Beroza & Ide, 2011; Rogers & Dragert, 2003). A renewal process models event occurrences in time, treating each new event occurrence as renewal in which the system is reset. It also assumes that inter-event times (i.e., the time between two consecutive events) are independent and identically distributed (Bebbington & Lai, 1996; Cruz-Reyna & Carrasco-Núñez, 2002). There are different types of renewal processes. For events that occur periodically or in clusters, Gamma or Weibull distributions are commonly used (Wang et al., 2024). In this work, we use renewal processes to characterize SSE occurrence patterns.

Our analysis focuses on SSEs located at the Hikurangi subduction zone, which marks the westward subduction of the Pacific plate beneath the Australian plate (Figure 1). Here, SSEs have been detected at shallow (<15 km) and deep (>20 km) depths along the plate interface (magenta contours in Figure 1). Shallow SSEs, located offshore the east coast of the North Island, last from 1 week to a few months and have moderate-to-large magnitudes (M_w5.9–7.0, Bartlow et al., 2014; Douglas et al., 2005; Wallace & Beavan, 2010; Woods et al., 2024). Deep SSEs have longer durations (1–2 years) than their shallower counterparts (e.g., Wallace, 2020; Wallace & Beavan, 2010; Wallace, Beavan, et al., 2012, 2018). Previous work suggest that the recurrence intervals of shallow Hikurangi SSEs vary along the margin (Wallace, 2020). However, these observations are limited due to an

incomplete event catalog. Additionally, it remains unclear whether SSE occurrence patterns were affected by 2016 M_w7.8 Kaikōura earthquake, which struck New Zealand's northeastern South Island (red star in Figure 1) rupturing more than 20 fault segments (thick red lines in Figure 1, after Hamling et al., 2017) and triggered widespread slow slip along the east coast and beneath the southern North Island (Wallace et al., 2017, 2018).

In this study, we introduce a statistical method to investigate the occurrence patterns of shallow Hikurangi SSEs. Note that we focus only on shallow SSEs, as only a few (<10) SSEs have occurred at deeper depths. Our study will help to characterize SSE behavior in a quantitative way.

2. Constructing SSE Catalog

To create a catalog of shallow Hikurangi SSEs, we analyzed time series data of GPS stations from the GeoNet network (orange triangles in Figure 1). Our analysis focuses on the period between 2006 and 2024, as few GPS stations had been installed before 2006. Over this period, many SSEs have been identified in the shallow SSE region (Bartlow et al., 2014; Delahaye et al., 2009; Ikari et al., 2020; Wallace & Beavan, 2010; Wallace & Eberhart-Phillips, 2013; Wallace et al., 2012a, 2018; Warren-Smith et al., 2019; Woods et al., 2022, 2024). To identify SSEs, we take advantage of the method developed by Ducellier et al. (2022), which uses wavelet analysis to highlight SSEs in GPS time series. This approach is complemented by manual picking of SSEs start and end times at GPS stations. An extended description of the methods to construct the catalog is given in the Text S1 and Figures S1–S7 of Supporting Information S1.

The SSE catalog, comprising 92 events, is shown in Figure 2a. Since most SSEs are detected at several stations, for simplicity, we only plot the earliest start time and latest end time for each event. In Figure 2a, we project the extension of the SSEs along the transect straddling the east coast of the North Island (black points in Figure 1). Note that the bottom and upper limits of each SSE correspond to the projected location along the transect of the northernmost and southernmost GPS station that recorded an event.

3. Assessing SSEs' Recurrence Patterns

3.1. Model Setup

We used statistical analysis to characterize the occurrence patterns of shallow Hikurangi SSEs in the catalog (Figure 2a). For simplicity, we only considered the start time of the SSE and its length. SSE length is defined by its extension along the transect (Figure 2a), which is approximated by the maximum distance along the transect between two GPS stations that detected an SSE. For SSEs that were only detected at one station, we assume that the length is equivalent to the minimum length of an SSE in the catalog, which is 1.5 km.

To characterize the spatial variation of SSE occurrence patterns along the margin, we divided the margin into different segments. The limits of the segments are defined based on the slip distribution of previous SSEs, which suggests that the SSE rupture areas tend to be segmented into four regions (e.g., Wallace, 2020; Wallace, Beavan, et al., 2012; Wallace et al., 2016, 2018). The extent of each segment is shown in Figure 1 (green dashed lines), and correspond from north to south to Tolaga Bay, Gisborne, Hawkes Bay and Cape Turnagain segments. Note that we considered alternative segmentation in Section 3.4. We do not include in the analysis SSEs occurring south of Cape Turnagain segment (Figure 1), as very few SSEs (<3) have been detected in this region, where the plate boundary is dominated by interseismic coupling (Wallace et al., 2004).

We classified SSEs into segments based on the following criteria. The SSE is assigned to the segments (a) where the station that recorded the maximum displacement is located, (b) where at least 50% (ΔL) of the SSE length is located, or where at least ΔL of the length of the segment slipped during the SSE. If either criterion (a) or (b) is satisfied in more than one segment, the SSE is classified as a multisegment SSE. Figure 2b shows the classification of SSEs into segments. In Section 3.4, we explore the sensitivity of the model results to variations in ΔL threshold.

3.2. Marked Renewal Process

We modeled SSE occurrence using a marked renewal process, in which the start time of an SSE is treated as an event occurrence and its length as a mark. SSE start time and SSE length are modeled independently, as empirical analysis indicates that they do not seem to be correlated (Figure S8 in Supporting Information S1). To model

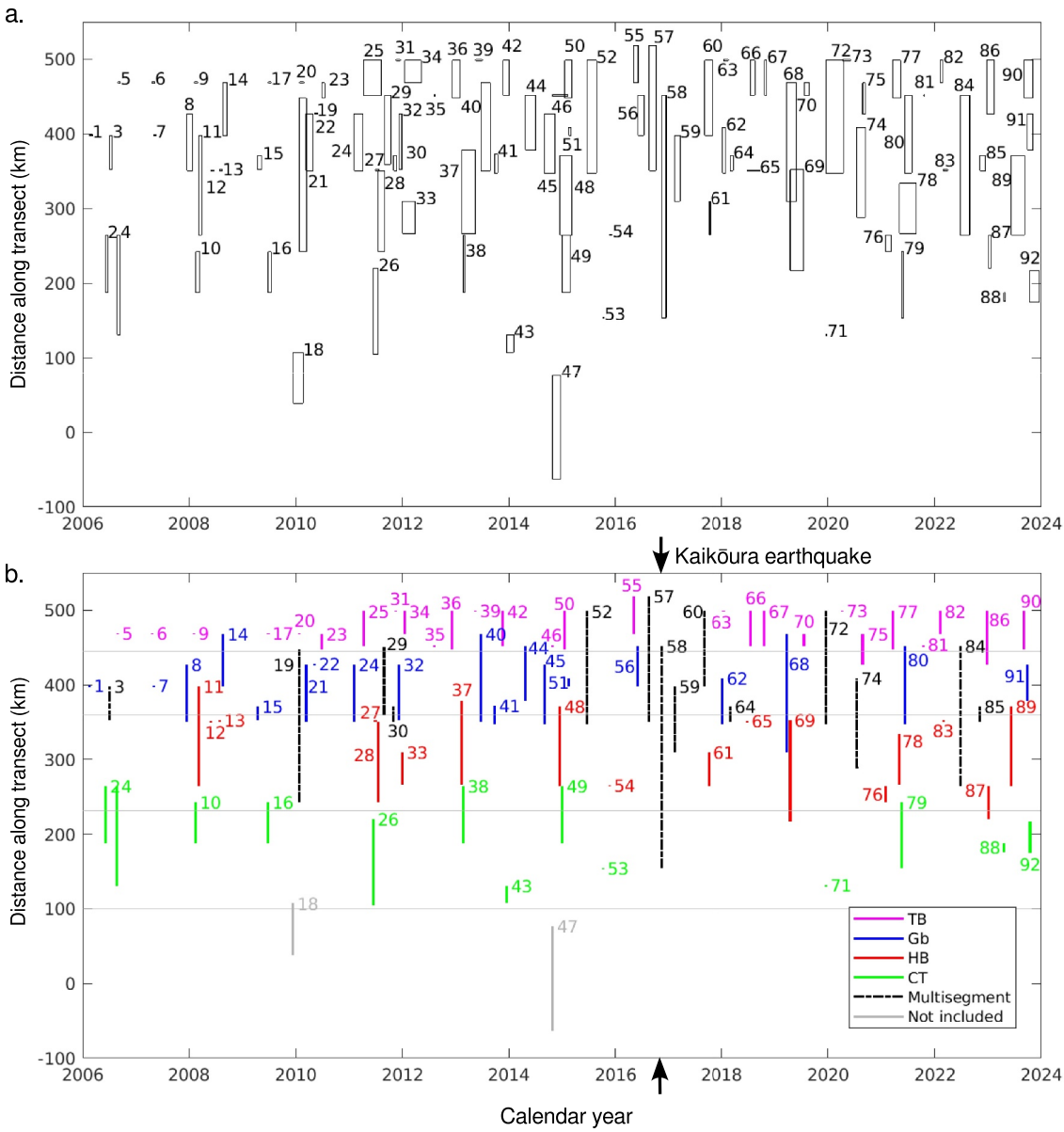

Figure 2. (a) Start and end times of all SSEs (labeled by event number) identified in this study and their extent along the transect (black circles in Figure 1). (b) Same as (a) but only showing start time and along-transect extent of SSEs. Horizontal gray lines indicate the segment boundaries (Figure 1). Colors indicate the segment where an SSE belongs, as shown in the legend, where TB, Gb, HB and CT stand for Tolaga Bay, Gisborne, Hawkes Bay and Cape Turnagain segments, respectively. Multisegment SSEs refer to events that rupture more than one segment along the margin. SSEs 18 and 47 are not included in the analysis (see text for details). Black arrows indicate the occurrence time of M_w7.8 Kaikōura earthquake.

SSEs, we consider the gamma distribution, as it is well-suited for describing periodic event occurrences (Wang et al., 2024). The intensity function describes the instantaneous rate of SSE occurrence with mark m at time t, as follows:

$$\delta(t,m) = \delta(t)g(m) \tag{1}$$

where $\delta(t) = f(t-s)/1 - F(t-s)$ is the intensity of a gamma renewal process with $f(t)$ being the probability density function, $F(t)$ the cumulative density function of a gamma distribution, t the start time of the SSE and s the start time of the last SSE before t. $g(m)$ is the probability density function of SSE length, which also follows a gamma distribution. For the ith segment:

$$\delta_i(t) \sim \frac{\lambda_i^{\nu_i}}{\Gamma(\nu_i)} t^{\nu_i - 1} e^{-\lambda_i t} \qquad g_i(m) \sim \frac{\beta_i^{\alpha_i}}{\Gamma(\alpha_i)} m^{\alpha_i - 1} e^{-\beta_i m} \tag{2}$$

where Γ is the gamma function, $\nu_i > 0$ and $\alpha_i > 0$ are the shape parameters, $\lambda_i > 0$ and $\beta_i > 0$ the rate and scale parameters, and $i = 1, 2, 3$, or 4 correspond to Tolaga Bay, Gisborne, Hawkes Bay and Cape Turnagain segments, respectively. For SSE occurrence in time, the shape parameter ν controls the degree of clustering or periodicity, with values below 1 indicative of clustering and above 1 of periodic behavior. The distribution of SSE lengths can be characterized by the coefficient of variation (CV) of $g(m)$, —given by $1/\sqrt{\alpha}$ for a gamma distribution—which indicates the level of dispersion of the distribution around the mean. A CV of $g(m)$ larger than 1 indicates a large dispersion of the distribution, values less than 1 point to low dispersion and a CV equal to 1 implies an exponential distribution, where the standard deviation is equal to the mean. The ratios ν/λ and α/β describe the distribution of the mean SSE recurrence time and the mean SSE length, respectively.

To compare the gamma distribution with alternative distributions (Weibull and lognormal), we used the Watanabe–Akaike information criterion (Text S2 in Supporting Information S1). Our results indicate that the WAIC of the Weibull distribution is close to that of the gamma distribution and could also be a suitable choice for describing SSE occurrence (Table S3 in Supporting Information S1).

We used Bayesian methods to estimate the posterior distribution (PD) of the model parameters. A Markov chain Monte Carlo (MCMC) algorithm generates samples from the joint PD of ν_i, λ_i, α_i and β_i, using software JAGS and R2jags package in *R* (Su & Yajima, 2012). We used weakly informative truncated-normal prior distributions for the parameters ν_i, λ_i, α_i and β_i, where each followed a half-normal distribution with a large variance, $N\left(0, 10^{-4}\right) T(0,)$. This choice is appropriate for small sample sizes (Gelman, 2006).

For the MCMC algorithm, we used three chains with 11,000 iterations, discarding the first 1,000 iterations as burn-in, and use a thinning rate of 20. The scale reduction factors of the Gelman-Rubin convergence diagnostic are all less than 1.02, indicating convergence (S. P. Brooks & Gelman, 1998; Gelman & Rubin, 1992).

3.3. Reference Model Results

To characterize SSE occurrence patterns, we considered two cases. For Case 1, we examined SSE occurrence at each segment over the entire time interval from 2006 to 2024. For Case 2, we divided the analysis into two time intervals, the first one from 2006 until M_w7.8 Kaikōura earthquake on 13 November 2016 UT (black arrows in Figure 2b), and the second one from the date of the earthquake until 2024. Note that SSE 58 (Figure 2) was triggered by the Kaikōura earthquake (Wallace et al., 2017, 2018).

The PD of parameters ν, ν/λ, CV of $g(m)$ and α/β for each segment in Case 1 are shown in Figures 3a–3d. We also calculated the highest posterior density (HPD) interval, which is the shortest interval containing the most probable values for each model parameter. In other words, every parameter value within the HPD has a higher PD than every value outside it (Gelman et al., 2013). A 95% HPD interval, indicating that there is a 95% probability that the true parameter value lies within that interval, is provided in Table S1 of Supporting Information S1. Notably, the HPD of shape parameter ν is above 1 in all segments (Table S1 in Supporting Information S1), indicating a quasi-periodic pattern. The PD of the mean recurrence interval ν/λ ranges from ~0.5 years to ~2 years, with noticeably larger values in Cape Turnagain segment (Figure 3b). The patterns of SSE lengths are indicated by the CV of $g(m)$ and α/β. The PD of CV takes relatively large values (~0.7 to 2, Figure 3c), with the 95% HPD interval including 1 in most segments (Table S1 in Supporting Information S1), which indicates an exponential SSE length distribution. The mean SSE length, indicated by α/β, ranges from tens of km to less than 150 km (Figure 3d) with lower values in Tolaga Bay segment (95% HPD interval of 25.7–61.7 km, Table S1 in Supporting Information S1).

To quantify the difference in the PD of model parameters across segments, we calculated the proportion of overlap between PDs for each parameter. An overlap of 1 indicates identical PDs, while an overlap of 0 implies no similarity between them. We set a threshold of 0.2, such that if the overlap falls below this threshold, we consider the difference between PDs to be significant (Wang et al., 2022). For Case 1, the overlap between PDs is shown in Figures 3e–3h (red horizontal line indicates the threshold). We found four significant features in the PD of model parameters. (a) SSE occurrence is more periodic (larger values of shape parameter ν) in Tolaga Bay segment (with

10.1029/2025GL116605

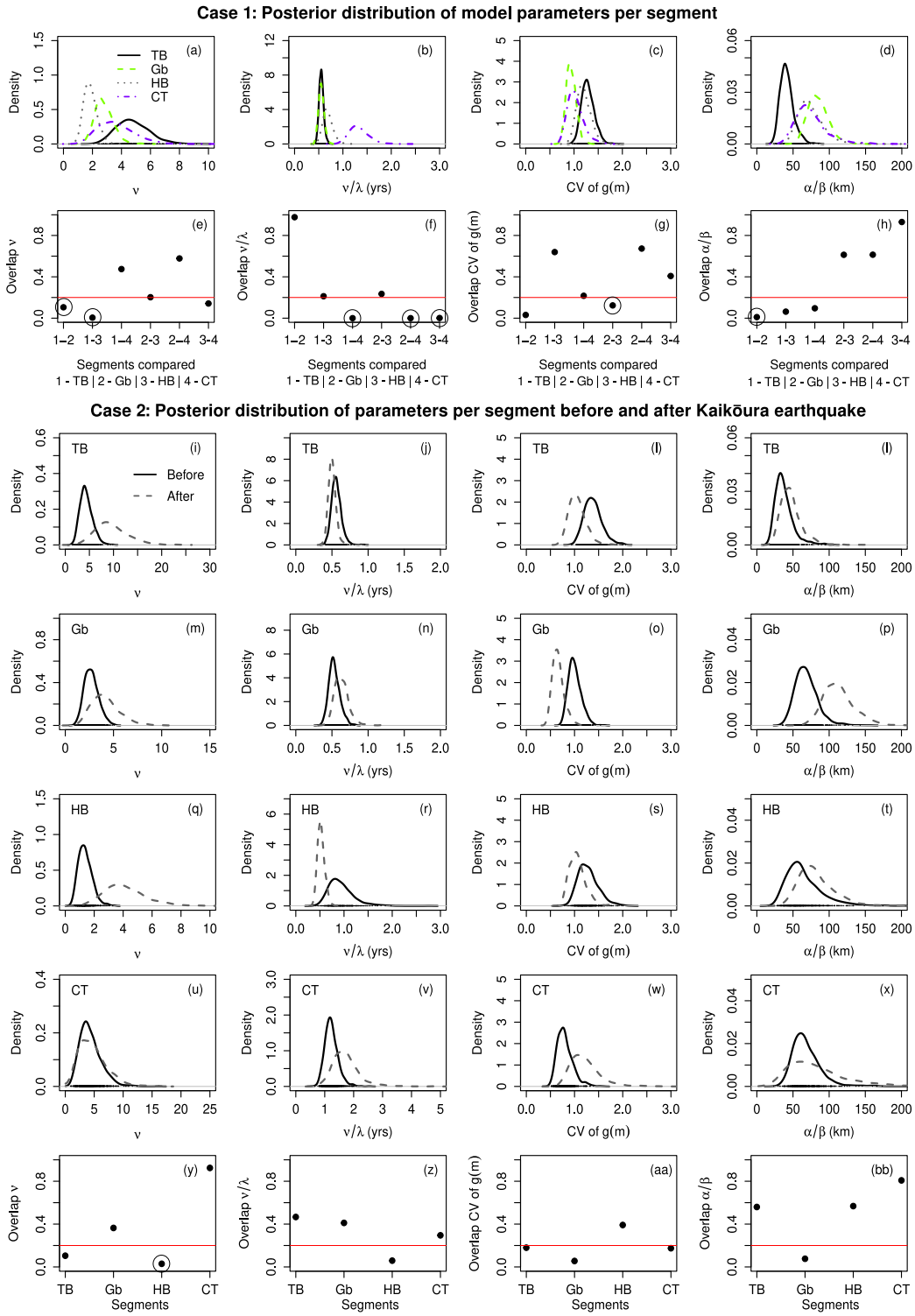

Figure 3. Results for reference model (Section 3.3). Posterior distributions of ν, ν/λ, α and α/β for (a–d) each segment in Case 1 and (i–x) before (solid black line) and after (dashed gray line) Kaikōura earthquake for segment (i–l) Tolaga Bay, (m–p) Gisborne, (q–t) Hawkes Bay and (u–x) Cape Turnagain (Case 2). (e–h) Overlap between posterior distributions for Case 1, *x*-axis label indicates the segments compared, where 1, 2, 3, 4 refer to Tolaga Bay (TB), Gisborne (Gb), Hawkes Bay (HB) and Cape Turnagain (CT) segments, respectively. (y–bb) Overlap between posterior distributions for each segment before and after Kaikōura earthquake. Red line in (e–h) and (y–bb) indicates the threshold of 0.2. Encircled dots in (e–h) and (y–bb) indicate the significant changes (overlap <0.2) that hold after accounting for Scenarios 1 and 2 (Section 3.4).

95% HPD of $\nu_1 > 2$, Table S1 in Supporting Information S1) compared to the central segments, Gisborne and Hawkes Bay (Figures 3a and 3e). SSEs in Cape Turnagain segment are significantly more periodic than SSEs in Hawkes Bay Segment (Figures 3a and 3e). (b) The mean recurrence interval, indicated by ν/λ, is significantly larger for Cape Turnagain segment than for the rest of the segments (Figures 3b and 3f). (c) The CV of SSE length distribution $g(m)$ indicates significantly lower dispersion of SSE lengths in Gisborne segment compared to Tolaga Bay and Hawkes Bay segment (Figures 3c and 3g). (d) SSE mean length is significantly lower for Tolaga Bay segment compared to the rest of the segments (Figures 3d and 3h in Supporting Information S1). We also calculate SSE length distribution and forecast of next SSE occurrence (Figure S9 in Supporting Information S1). We conduct a residual analysis (Wang et al., 2019, 2022) to evaluate the goodness-of-fit of the model. Our results indicate that the model provides a good fit to the data (Figures S10 and S11 in Supporting Information S1). However, the fit of the distribution is less optimal for short SSEs lengths (Figure S11 in Supporting Information S1).

In Case 2, we compared the PD of each model parameter (ν, ν/λ, CV of $g(m)$ and α/β) before and after the Kaikōura earthquake for each segment, as shown in Figures 3i–3x. The overlap between PDs is shown in Figures 3y–3bb. To assess the effect of Kaikōura earthquake, we also forecast the occurrence time of the first four SSEs at each segment after the earthquake. Our results indicate that the observed SSE occurrence times fall within the 95% HPD interval predicted by our model (Figure S12 in Supporting Information S1).

3.4. Sensitivity of Model Results

To assess the sensitivity of the results to some of our modeling assumptions, we analyzed three alternative scenarios, in which we considered: Alternative thresholds ΔL to classify SSEs into segments (Scenario 1), more robust SSE detections (Scenario 2), and a different division of the margin into segments (Scenario 3). An extended description of these scenarios is given in the Text S3 of Supporting Information S1. The results for these cases are shown in Figures S13–S16 of Supporting Information S1. For comparison, we highlight the common significant features (overlap < 0.2) between these scenarios and the reference model (encircled dots in Figures 3e–3h and 3y–3bb). For Case 1, most of the significant features in reference model hold. For Case 2, only one holds: SSEs are more periodic (larger ν values) after the earthquake in Hawkes Bay segment (Figure 3q and encircled dot in Figure 3y).

3.5. Analysis of SSE Occurrence Patterns at Individual GPS Stations

We examined SSE occurrence patterns at individual GPS stations to assess whether the spatial trends in our reference model align with those observed at stations located in the same regions. Only stations closest to the east coast of the North Island (stations labeled in Figure 1) were considered in the analysis, as they have a better record of shallow SSEs.

To characterize SSE occurrence, we model SSE start time by means of the intensity $\delta(t)$ at each station (Equation 1); excluding SSE length $g(m)$, as it cannot be constrained at a single station. We show the PD of model parameters that describe SSE occurrence pattern (ν) and SSE recurrence interval (ν/λ) for each station in Figure 4 with stations grouped by segment (see also Table S2 in Supporting Information S1). Consistent with the reference model (Figure 3), the PD of the shape parameter ν takes larger values for stations located in Tolaga Bay segment (Figure 4a), indicating more periodic SSE occurrence. Similarly, the PD of ν/λ indicates longer recurrence intervals for stations in Cape Turnagain segment (Figure 4h), and shorter recurrence for stations in Tolaga Bay and Gisborne segments (Figures 4b and 4d). Model parameters for stations in Hawkes Bay segment (Figures 4e and 4f) exhibit larger variability. For instance, the PD of ν/λ for station MAHI indicates shorter inter-arrival times (<1 yr) compared to other stations in the same segment (Figure 4f). This can be explained by the location of station MAHI, which sits close to the boundary between Gisborne and Hawkes Bay segments (Figure 1) and records SSEs from both segments.

To determine the effect of Kaikōura earthquake on SSE occurrence at each station, we also examined the PD of model parameters ν and ν/λ before and after the earthquake. However, we found no consistent trends in the change of PDs for stations located in the same segment (Figures S20–S23 in Supporting Information S1).

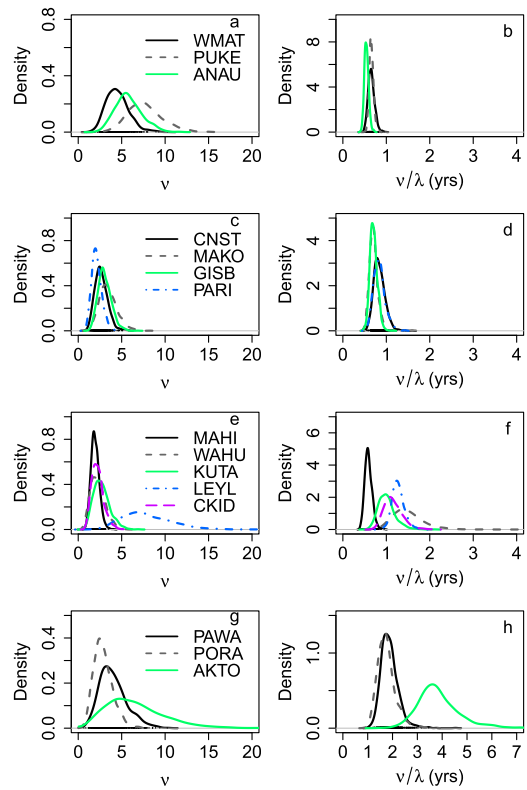

Figure 4. Posterior distribution of model parameters ν and ν/λ at individual GPS stations along the coast (see station labeled in Figure 1). Stations are grouped by segments: (a–b) Tolaga Bay, (c–d) Gisborne, (e–f) Hawkes Bay and (g–h) Cape Turnagain. Note that we do not include station CAST due to the low number of SSEs (<4) recorded at that station.

4. Discussion

4.1. Segmentation of SSE Recurrence Intervals

Our results indicate that the recurrence intervals of shallow SSEs vary significantly along the Hikurangi margin (Figures 3b and 3f). In the southern part of the margin (Cape Turnagain segment), SSEs occur less frequently, with 95% HPD range of 0.95–1.72 years (Table S1 in Supporting Information S1). In contrast, SSEs are more frequent in the northern part of the margin (Tolaga Bay and Gisborne segments), with a 95% HPD range of 0.45–0.68 years (Table S1 in Supporting Information S1). These trends persist across different scenarios (Section 3.4) and in the analysis of SSE recurrence at individual GPS stations (Figure 4), although there is some variability between stations within the same segment. Overall, our model results are consistent with Wallace (2020). However, our analysis indicates shorter SSE recurrence intervals than estimated by Wallace (2020), which we attribute to the inclusion of smaller SSEs in our catalog. It is important to note that our model results rely on an SSE catalog constrained solely by inland GPS stations, which have limited detection capability offshore, where most of the slip of shallow Hikurangi SSEs concentrates (e.g., Wallace, 2020; Wallace & Beavan, 2010). In addition, the irregular distribution of stations over time (i.e., more stations in later years) and along the margin (i.e., stations closer to SSE source region in the north, Figure 1) may lead to differences in detectability in time and space. Thus, it is plausible that the denser and more favorably located stations in the northern part of the margin enables the detection of smaller SSEs that may go unnoticed elsewhere. Future work incorporating seafloor geodetic data (e.g., Woods et al., 2022; Woods et al., 2024) may be necessary to assess the model predictions.

The factors driving changes in shallow SSE recurrence intervals along the Hikurangi margin remain poorly understood. Using numerical simulations, Perez-Silva et al. (2022) suggested that along-strike changes in the plate dip angle and the plate convergence rate, both lower in the southern part of the margin (Wallace et al., 2004; Williams et al., 2013), contribute to the longer recurrence intervals of SSEs in that region. Further research is needed to determine whether other factors, such as along-strike changes in the megathrust protolith (Gase

et al., 2022), in the level of pore fluid pressure (Bangs et al., 2023; Chesley et al., 2021; Gase et al., 2023) and in the structure of the upper plate (Bassett et al., 2022) may also play a role.

4.2. Spatiotemporal SSE Occurrence Patterns and Influence of Kaikōura Earthquake

Temporal SSE occurrence patterns are generally characterized as quasi-periodic, a description supported by our quantitative results. The PD of shape parameter ν suggests that SSE occurrence tends to be quasi-periodic, as the 95% HPD interval is larger than 1 across all segments (Table S1 in Supporting Information S1). Additionally, our findings reveal spatial variations in SSE periodicity along the Hikurangi margin. SSE occurrence is most regular in Tolaga Bay segment, where shape parameter ν takes larger values (with 95% HPD interval for ν_1 (2.6, 6.9), Table S1 in Supporting Information S1), followed by Cape Turnagain segment (ν_4 (1.4, 6.1) in Table S1 in Supporting Information S1). For the central segments, Gisborne and Hawkes Bay, SSE occurrence is less periodic, with lower values for ν (95% HPD interval of ν_2 and ν_3 is (1.6, 4), Table S1 in Supporting Information S1).

Our model results suggest that SSE length distribution ranges from tens of km to over a 100 km with some variability across segments, though most differences are not statistically significant (Figure 3d and Table S1 in Supporting Information S1). The only significant difference is that SSEs in Tolaga Bay segment are shorter than those in Gisborne segment (Figures 3d and 3h, and Table S1 and Figure S9 in Supporting Information S1). The variability of SSE lengths could be due to the heterogeneous nature of the source region of shallow Hikurangi SSEs, which manifests as lithological, geometrical and rheological changes observed at length scales ranging from centimeters to kilometers (Barnes et al., 2020). We also find that the exponential distribution is a good description of SSE length distribution in the reference model (95% HPD interval of CV of $g(m)$ includes 1, Table S1 in Supporting Information S1) in most of the margin (Gisborne, Hawkes Bay and Cape Turnagain segments), which implies that most SSE lengths are short while occasionally long SSEs occur. However, the exponential model fits less well for the shortest SSEs (Figure S11 in Supporting Information S1), for which a minimum length was assumed. In addition, the distribution does not fit the data well in Scenario 2 (Section 3.4), where the shortest SSEs were excluded (Text S3 in Supporting Information S1). These limitations highlight the need for improved constraints on SSE lengths to better characterize their distribution.

Our results do not provide conclusive evidence of the Kaikōura earthquake's impact on SSE occurrence patterns. Most of the significant features found in the reference model (overlap < 0.2 in Figures 3y and 3xx) depend on some of the modeling assumptions (Section 3.4 and Text S2 in Supporting Information S1) and are not visible when examining individual GPS stations (Section 3.5). In addition, our forecast indicates that SSE occurrence did not significantly change after the earthquake (Figure S12 in Supporting Information S1). At most, our results suggest that the effect of the earthquake may have been transient, as evidenced by the SSEs triggered by it (Wallace et al., 2018).

5. Conclusions

We used renewal processes to investigate the occurrence patterns of SSEs that occur along the shallow portion of the Hikurangi margin. First, we constructed a catalog of these events that constrains their timing and along-strike extent. Second, we modeled the occurrence patterns of SSEs in the catalog as a marked renewal process, using Bayesian inference to obtain the posterior distributions of the model parameters. Our model results indicate that SSE recurrence intervals vary along the margin, with less frequent events occurring in the southern part of the margin, offshore Cape Turnagain and more frequent events in the northern part of the margin, offshore Tolaga Bay and Gisborne regions. Additionally, we find that SSE occurrence patterns are generally quasi-periodic throughout the margin. The regularity of SSE occurrence also varies spatially, with SSEs occurring most regularly in the northern part of the margin. Finally, we do not find conclusive evidence that the 2016 M_w7.8 Kaikōura earthquake had a lasting effect on SSE occurrence patterns.

Data Availability Statement

Data set of SSE catalog and scripts to model renewal processes are archived in a Zenodo repository (Perez-Silva et al., 2025).

Acknowledgments
A.P-S., T.W. and L.W. are funded by MBIE Endeavour Fund (Smart Ideas, Grant UOOX2206). ChatGPT was used for language editing throughout the manuscript. Open access publishing facilitated by University of Otago, as part of the Wiley - University of Otago agreement via the Council of Australian University Librarians.

References

Audet, P., & Bürgmann, R. (2014). Possible control of subduction zone slow-earthquake periodicity by silica enrichment. *Nature*, *510*(7505), 389–392. https://doi.org/10.1038/nature13391

Bangs, N. L., Morgan, J. K., Bell, R. E., Han, S., Arai, R., Kodaira, S., et al. (2023). Slow slip along the Hikurangi margin linked to fluid-rich sediments trailing subducting seamounts. *Nature Geoscience*, *16*(6), 505–512. https://doi.org/10.1038/s41561-023-01186-3

Barnes, P. M., Wallace, L. M., Saffer, D. M., Bell, R. E., Underwood, M. B., Fagereng, Å., et al. (2020). Slow slip source characterized by lithological and geometric heterogeneity. *Science Advances*, *6*(13), eaay3314. https://doi.org/10.1126/sciadv.aay3314

Bartlow, N. M., Wallace, L. M., Beavan, R. J., Bannister, S., & Segall, P. (2014). Time-dependent modeling of slow slip events and associated seismicity and tremor at the Hikurangi subduction zone, New Zealand. *Journal of Geophysical Research: Solid Earth*, *119*(1), 734–753. https://doi.org/10.1002/2013JB010609

Bassett, D., Arnulf, A., Henrys, S., Barker, D., Avendonk, H., Bangs, N., et al. (2022). Crustal structure of the Hikurangi margin from SHIRE seismic data and the relationship between forearc structure and shallow megathrust slip behavior. *Geophysical Research Letters*, *49*(2), e2021GL096960. https://doi.org/10.1029/2021GL096960

Bebbington, M. S., & Lai, C. D. (1996). On nonhomogeneous models for volcanic eruptions. *Mathematical Geology*, *28*(5), 585–600. https://doi.org/10.1007/BF02066102

Beroza, G. C., & Ide, S. (2011). Slow earthquakes and nonvolcanic tremor. *Annual Review of Earth and Planetary Sciences*, *39*(1), 271–296. https://doi.org/10.1146/annurev-earth-040809-152531

Brooks, B., Foster, J. H., Bevis, M., Frazer, L. N., Wolfe, C. J., & Behn, M. (2006). Periodic slow earthquakes on the flank of Kīlauea volcano, Hawaii. *Earth and Planetary Science Letters*, *246*(3–4), 207–216. https://doi.org/10.1016/j.epsl.2006.03.035

Brooks, S. P., & Gelman, A. (1998). General methods for monitoring convergence of iterative simulations. *Journal of Computational & Graphical Statistics*, *7*(4), 434–455. https://doi.org/10.1080/10618600.1998.10474787

Brudzinski, M. R., & Allen, R. M. (2007). Segmentation in episodic tremor and slip all along Cascadia. *Geology*, *35*(10), 907–910. https://doi.org/10.1130/G23740A.1

Chesley, C., Naif, S., Key, K., & Bassett, D. (2021). Fluid-rich subducting topography generates anomalous forearc porosity. *Nature*, *595*(7866), 255–260. https://doi.org/10.1038/s41586-021-03619-8

Cruz-Atienza, V. M., Tago, J., Villafuerte, C., Wei, M., Garza-Girón, R., Dominguez, L. A., et al. (2021). Short-term interaction between silent and devastating earthquakes in Mexico. *Nature Communications*, *12*(1), 2171. https://doi.org/10.1038/s41467-021-22326-6

Cruz-Reyna, S., & Carrasco-Núñez, G. (2002). Probabilistic hazard analysis of Citlaltépetl (Pico de Orizaba) Volcano, eastern Mexican Volcanic Belt. *Journal of Volcanology and Geothermal Research*, *113*(1–2), 307–318. https://doi.org/10.1016/S0377-0273(01)00263-3

Delahaye, E., Townend, J., Reyners, M., & Rogers, G. (2009). Microseismicity but no tremor accompanying slow slip in the Hikurangi subduction zone, New Zealand. *Earth and Planetary Science Letters*, *277*(1–2), 21–28. https://doi.org/10.1016/j.epsl.2008.09.038

Dixon, T. H., Jiang, Y., Malservisi, R., McCaffrey, R., Voss, N., Protti, M., & Gonzalez, V. (2014). Earthquake and tsunami forecasts: Relation of slow slip events to subsequent earthquake rupture. *Proceedings of the National Academy of Sciences USA*, *111*(48), 17039–17044. https://doi.org/10.1073/pnas.1412299111

Douglas, A., Beavan, J., Wallace, L., & Townend, J. (2005). Slow slip on the northern Hikurangi subduction interface, New Zealand. *Geophysical Research Letters*, *32*(16), L16305. https://doi.org/10.1029/2005GL023607

Dragert, H., Wang, K., & James, T. S. (2001). A silent slip event on the deeper Cascadia subduction interface. *Science*, *292*(5521), 1525–1528. https://doi.org/10.1126/science.1060152

Ducellier, A., Creager, K. C., & Schmidt, D. A. (2022). Detection of slow slip events using wavelet analysis of GNSS recordings. *Bulletin of the Seismological Society of America*, *112*(5), 2408–2424. https://doi.org/10.1785/0120210289

Fu, Y., Liu, Z., & Freymueller, J. T. (2015). Spatiotemporal variations of the slow slip event between 2008 and 2013 in the southcentral Alaska subduction zone. *Geochemistry, Geophysics, Geosystems*, *16*(7), 2450–2461. https://doi.org/10.1002/2015GC005904

Gase, A. C., Bangs, N. L., Avendonk, H. J. V., Bassett, D., & Henrys, S. A. (2022). Hikurangi megathrust slip behavior influenced by lateral variability in sediment subduction. *Geology*, *50*(10), 1145–1149. https://doi.org/10.1130/G50261.1

Gase, A. C., Bangs, N. L., Saffer, D. M., Han, S., Miller, P. K., Bell, R. E., et al. (2023). Subducting volcaniclastic-rich upper crust supplies fluids for shallow megathrust and slow slip. *Science Advances*, *9*(33), eadh0150. https://doi.org/10.1126/sciadv.adh0150

Gelman, A. (2006). Prior distributions for variance parameters in hierarchical models. *Bayesian Analysis*, *1*(3). https://doi.org/10.1214/06-BA117A

Gelman, A., Carlin, J. B., Stern, H. S., Dunson, D. B., Vehtari, A., & Rubin, D. B. (2013). *Bayesian data analysis*. Chapman and Hall/CRC. https://doi.org/10.1201/b16018

Gelman, A., & Rubin, D. B. (1992). Inference from iterative simulation using multiple sequences. *Statistical Science*, *7*(4), 457–472. https://doi.org/10.1214/ss/1177011136

Graham, S., DeMets, C., Cabral-Cano, E., Kostoglodov, V., Rousset, B., Walpersdorf, A., et al. (2016). Slow slip history for the Mexico subduction zone: 2005 through 2011. *Pure and Applied Geophysics*, *173*, 3445–3465. https://doi.org/10.1007/978-3-319-51529-8_13

Hamling, I. J., Hreinsdóttir, S., Clark, K., Elliott, J., Liang, C., Fielding, E., et al. (2017). Complex multifault rupture during the 2016 M_w 7.8 Kaikōura earthquake, New Zealand. *Science*, *356*(6334). https://doi.org/10.1126/science.aam7194

Hirose, H., Hirahara, K., Kimata, F., Fujii, N., & Miyazaki, S. (1999). A slow thrust slip event following the two 1996 Hyuganada earthquakes beneath the Bungo Channel, Southwest Japan. *Geophysical Research Letters*, *26*(21), 3237–3240. https://doi.org/10.1029/1999GL010999

Ide, S., & Nomura, S. (2022). Forecasting tectonic tremor activity using a renewal process model. *Progress in Earth and Planetary Science*, *9*(1), 67. https://doi.org/10.1186/s40645-022-00523-1

Ikari, M. J., Wallace, L. M., Rabinowitz, H. S., Savage, H. M., Hamling, I. J., & Kopf, A. J. (2020). Observations of laboratory and natural slow slip events: Hikurangi subduction zone, New Zealand. *Geochemistry, Geophysics, Geosystems*, *21*(2), e2019GC008717. https://doi.org/10.1029/2019GC008717

Matthews, M. V., Ellsworth, W. L., & Reasenberg, P. A. (2002). A Brownian model for recurrent earthquakes. *Bulletin of the Seismological Society of America*, *92*(6), 2233–2250. https://doi.org/10.1785/0120010267

Nishimura, T. (2014). Short-term slow slip events along the Ryukyu Trench, southwestern Japan, observed by continuous GNSS. *Progress in Earth and Planetary Science*, *1*, 22. https://doi.org/10.1186/s40645-014-0022-5

Nomura, S., Ogata, Y., Komaki, F., & Toda, S. (2011). Bayesian forecasting of recurrent earthquakes and predictive performance for a small sample size. *Journal of Geophysical Research*, *116*(B4), B04315. https://doi.org/10.1029/2010JB007917

Ogata, Y. (1999). Estimating the hazard of rupture using uncertain occurrence times of paleoearthquakes. *Journal of Geophysical Research*, *104*(B8), 17995–18014. https://doi.org/10.1029/1999JB900115

Ozawa, S. (2014). Shortening of recurrence interval of Boso slow slip events in Japan. *Geophysical Research Letters*, *41*(8), 2762–2768. https://doi.org/10.1002/2014GL060072

Perez-Silva, A., Kaneko, Y., Savage, M., Wallace, L., Li, D., & Williams, C. (2022). Segmentation of shallow slow slip events at the Hikurangi subduction zone explained by along-strike changes in fault geometry and plate convergence rates. *Journal of Geophysical Research: Solid Earth*, *127*(1), e2021JB022913. https://doi.org/10.1029/2021JB022913

Perez-Silva, A., Wang, T., Wallace, L., Bebbington, M., & Denys, P. (2025). Data products for research paper titled: Assessing occurrence patterns of shallow Hikurangi slow slip events using renewal processes [Dataset]. *Zenodo*. https://doi.org/10.5281/zenodo.14848128

Radiguet, M., Cotton, F., Vergnolle, M., Campillo, M., Walpersdorf, A., Cotte, N., & Kostoglodov, V. (2012). Slow slip events and strain accumulation in the Guerrero gap, Mexico. *Journal of Geophysical Research*, *117*(B4), B04305. https://doi.org/10.1029/2011JB008801

Rogers, G., & Dragert, H. (2003). Episodic tremor and slip on the Cascadia subduction zone: The chatter of silent slip. *Science*, *300*(5627), 1942–1943. https://doi.org/10.1126/science.1084783

Rousset, B., Bürgmann, R., & Campillo, M. (2019). Slow slip events in the roots of the San Andreas Fault. *Science Advances*, *5*(2), eaav3274. https://doi.org/10.1126/sciadv.aav3274

Rousset, B., Campillo, M., Lasserre, C., Frank, W. B., Cotte, N., Walpersdorf, A., et al. (2017). A geodetic matched filter search for slow slip with application to the Mexico subduction zone. *Journal of Geophysical Research: Solid Earth*, *122*(12), 10498–10514. https://doi.org/10.1002/2017JB014448

Su, Y.-S., & Yajima, M. (2012). R2jags: A package for running jags from R. R package version 0.03–08.

Takagi, R., Uchida, N., & Obara, K. (2019). Along-strike variation and migration of long-term slow slip events in the western Nankai subduction zone, Japan. *Journal of Geophysical Research: Solid Earth*, *124*, 3853–3880. https://doi.org/10.1029/2019JB018037

Wallace, L. M. (2020). Slow slip events in New Zealand. *Annual Review of Earth and Planetary Sciences*, *48*(1), 175–203. https://doi.org/10.1146/annurev-earth-071719-055104

Wallace, L. M., Barnes, P., Beavan, J., Van Dissen, R., Litchfield, N., Mountjoy, J., et al. (2012). The kinematics of a transition from subduction to strike-slip: An example from the central New Zealand plate boundary. *Journal of Geophysical Research*, *117*(B2), B02405. https://doi.org/10.1029/2011JB008640

Wallace, L. M., & Beavan, J. (2010). Diverse slow slip behavior at the Hikurangi subduction margin, New Zealand. *Journal of Geophysical Research*, *115*(B12), B12402. https://doi.org/10.1029/2010JB007717

Wallace, L. M., Beavan, J., Bannister, S., & Williams, C. (2012). Simultaneous long-term and short-term slow slip events at the Hikurangi subduction margin, New Zealand: Implications for processes that control slow slip event occurrence, duration, and migration. *Journal of Geophysical Research*, *117*(B11), B11402. https://doi.org/10.1029/2012JB009489

Wallace, L. M., Beavan, J., McCaffrey, R., & Darby, D. (2004). Subduction zone coupling and tectonic block rotations in the North Island, New Zealand. *Journal of Geophysical Research*, *109*(B12), B12406. https://doi.org/10.1029/2004JB003241

Wallace, L. M., & Eberhart-Phillips, D. (2013). Newly observed, deep slow slip events at the central Hikurangi margin, New Zealand: Implications for downdip variability of slow slip and tremor, and relationship to seismic structure. *Geophysical Research Letters*, *40*(20), 5393–5398. https://doi.org/10.1002/2013GL057682

Wallace, L. M., Hreinsdóttir, S., Ellis, S., Hamling, I., D'Anastasio, E., & Denys, P. (2018). Triggered slow slip and afterslip on the southern Hikurangi subduction zone following the Kaikōura earthquake. *Geophysical Research Letters*, *45*, 4710–4718. https://doi.org/10.1002/2018GL077385

Wallace, L. M., Kaneko, Y., Hreinsdóttir, S., Hamling, I., Peng, Z., Bartlow, N., et al. (2017). Large-scale dynamic triggering of shallow slow slip enhanced by overlying sedimentary wedge. *Nature Geoscience*, *10*, 765–770. https://doi.org/10.1038/ngeo3021

Wallace, L. M., Webb, S. C., Ito, Y., Mochizuki, K., Hino, R., Henrys, S., et al. (2016). Slow slip near the trench at the Hikurangi subduction zone, New Zealand. *Science*, *352*(6286), 701–704. https://doi.org/10.1126/science.aaf2349

Wang, T., & Bebbington, M. (2012). Estimating the likelihood of an eruption from a volcano with missing onsets in its record. *Journal of Volcanology and Geothermal Research*, *243–244*, 14–23. https://doi.org/10.1016/j.jvolgeores.2012.06.032

Wang, T., Bebbington, M., Cronin, S., & Carman, J. (2022). Forecasting eruptions at poorly known volcanoes using analogs and multivariate renewal processes. *Geophysical Research Letters*, *49*(12). https://doi.org/10.1029/2021GL096715

Wang, T., Griffin, J. D., Brenna, M., Fletcher, D., Zeng, J., Stirling, M., et al. (2024). Earthquake forecasting from paleoseismic records. *Nature Communications*, *15*(1), 1944. https://doi.org/10.1038/s41467-024-46258-z

Wang, T., Schofield, M., Bebbington, M., & Kiyosugi, K. (2019). Bayesian modelling of marked point processes with incomplete records: Volcanic eruptions. *Journal of the Royal Statistical Society—Series C: Applied Statistics*, *69*(1), 109–130. https://doi.org/10.1111/rssc.12380

Warren-Smith, E., Fry, B., Wallace, L., Chon, E., Henrys, S., Sheehan, A., et al. (2019). Episodic stress and fluid pressure cycling in subducting oceanic crust during slow slip. *Nature Geoscience*, *12*(6), 475–481. https://doi.org/10.1038/s41561-019-0367-x

Wei, M., Sandwell, D., & Fialko, Y. (2009). A silent M_w 4.7 slip event of October 2006 on the Superstition Hills fault, southern California. *Journal of Geophysical Research*, *114*(B7), B07402. https://doi.org/10.1029/2008JB006135

Williams, C. A., Eberhart-Phillips, D., Bannister, S., Barker, D. H., Henrys, S., Reyners, M., & Sutherland, R. (2013). Revised interface geometry for the Hikurangi subduction zone, New Zealand. *Seismological Research Letters*, *84*(6), 1066–1073. https://doi.org/10.1785/0220130035

Woods, K., Wallace, L. M., Williams, C. A., Hamling, I. J., Webb, S. C., Ito, Y., et al. (2024). Spatiotemporal evolution of slow slip events at the offshore Hikurangi subduction zone in 2019 using GNSS, InSAR, and seafloor geodetic data. *Journal of Geophysical Research: Solid Earth*, *129*(8). https://doi.org/10.1029/2024JB029068

Woods, K., Webb, S. C., Wallace, L. M., Ito, Y., Collins, C., Palmer, N., et al. (2022). Using seafloor geodesy to detect vertical deformation at the Hikurangi Subduction Zone: Insights from self-calibrating pressure sensors and ocean general circulation models. *Journal of Geophysical Research: Solid Earth*, *127*(12), e2022JB023989. https://doi.org/10.1029/2022JB023989

References From the Supporting Information

Addison, P. S. (2002). *The illustrated wavelet transform handbook: Introductory theory and applications in science, engineering, medicine and finance*. Cambridge University Press.

Blewitt, G., Hammond, W., & Kreemer, C. (2018). Harnessing the GPS data explosion for interdisciplinary science. *Eos*, *99*. https://doi.org/10.1029/2018EO104623

Fasola, S. L., Jackson, N. M., & Williams, C. A. (2023). Deep short-term slow slip and tremor in the Manawatu region, New Zealand. *Geophysical Research Letters*, *50*(21). https://doi.org/10.1029/2023GL105428

Fletcher, D. (2018). *Model averaging*. Springer.

GNS. (2000). GeoNet Aotearoa New Zealand continuous GNSS network time series dataset [Dataset]. *GNS Science, GeoNet*. https://doi.org/10.21420/30F4-1A55

Nishimura, T., Matsuzawa, T., & Obara, K. (2013). Detection of short-term slow slip events along the Nankai Trough, southwest Japan, using GNSS data. *Journal of Geophysical Research: Solid Earth*, *118*(6), 3112–3125. https://doi.org/10.1002/jgrb.50222

Percival, D. B., & Walden, A. T. (2000). *Wavelet methods for time series analysis*. Cambridge University Press.

Watanabe, S. (2010). Asymptotic equivalence of Bayes cross validation and widely applicable information criterion in singular learning theory. *Journal of Machine Learning Research*, *11*, 3571–3594.

Wdowinski, S., Bock, Y., Zhang, J., Fang, P., & Genrich, J. (1997). Southern California permanent GPS geodetic array: Spatial filtering of daily positions for estimating coseismic and postseismic displacements induced by the 1992 Landers earthquake. *Journal of Geophysical Research*, *102*(B8), 18057–18070. https://doi.org/10.1029/97jb01378